



Hurricane Matthew in 2100: effects of extreme sea level rise scenarios on a highly valued coastal area (Palm Beach, FL, USA)

Patrick Boyden¹ · Elisa Casella² · Christopher Daly³ · Alessio Rovere¹

Received: 23 March 2021 / Accepted: 16 August 2021 / Published online: 8 September 2021
© The Author(s) 2021

Abstract

Sea-level rise represents a severe hazard for populations living within low-elevation coastal zones and is already largely affecting coastal communities worldwide. As sea level continues to rise following unabated greenhouse gas emissions, the exposure of coastal communities to inundation and erosion will increase exponentially. These impacts will be further magnified under extreme storm conditions. In this paper, we focus on one of the most valuable coastal real estate markets globally (Palm Beach, FL). We use XBeach, an open-source hydro and morphodynamic model, to assess the impact of a major tropical cyclone (Hurricane Matthew, 2016) under three different sea-level scenarios. The first scenario (modern sea level) serves as a baseline against which other model runs are evaluated. The other two runs use different 2100 sea-level projections, localized to the study site: (i) IPCC RCP 8.5 (0.83 m by 2100) and (ii) same as (i), but including enhanced Antarctic ice loss (1.62 m by 2100). Our results show that the effective doubling of future sea level under heightened Antarctic ice loss amplifies flow velocity and wave height, leading to a 46% increase in eroded beach volume and the overtopping of coastal protection structures. This further exacerbates the vulnerability of coastal properties on the island, leading to significant increases in parcel inundation.

Introduction

Human development is disproportionately concentrated around coastal trading hubs. Between 94 million and 150 million people are currently living within areas at risk of inundation under future sea-level rise by the year 2100 (Kopp et al. 2017). This number is expected to grow as low-lying coastal regions see continued population expansion. For example, Neumann et al. (2015) calculated that over 411 million people could be exposed to the 100-year coastal flood plain by 2060.

By 2100, global mean sea level (GMSL) is expected to rise between approximately 0.43 and 0.84 m under

Representative Concentration Pathways (RCP) 2.6 and 8.5, respectively (Pörtner et al. 2019). Within these predictions, debate persists as to the amount in which ice sheets will contribute to GMSL rise in the future. Central to projecting future GMSL is the understanding of processes dictating marine ice-shelf and marine ice-cliff (in)stability under warmer climate conditions (Oppenheimer and Alley 2016). DeConto and Pollard (2016) propose that hydrofracturing and ice-sheet calving of the Antarctic Ice Sheet (AIS) would create a runaway ice-shelf retreat under warm atmospheric and ocean temperatures, resulting in more than a 1-m contribution to GMSL from the AIS in 2100. However, the physical processes still have significant uncertainties, and some studies have shown the possibility to fit geological constraints without ice-shelf and ice-cliff instability (Edwards et al. 2019).

Moreover, several processes may affect the local magnitude of sea level changes. For example, land motions through time may be caused by glacial isostatic adjustment (Davis and Mitrovica 1996) or subsidence (Törnqvist et al. 2008). These processes cause local sea level to depart from GMSL, and may exacerbate the impact of sea-level rise. To account for these effects, Kopp et al. (2014) and Kopp

✉ Patrick Boyden
pboyden@marum.de

¹ MARUM - Center for Marine Environmental Sciences, University of Bremen, Bremen, Germany

² ZMT - Leibniz Center for Tropical Marine Research, Bremen, Germany

³ Leiden University College, Leiden, The Netherlands

et al. (2017) provided a method to localize different GMSL projections for the majority of Permanent Service for Mean Sea Level (PSMSL) tidal stations.

In addition to GMSL rise and local effects, low-lying coastal zones in the lower latitudes face a further threat: tropical cyclones. These affect sea level at short time scales as storm surge, driven by wind and pressure at the cyclone front, produces a locally heightened sea level that can be in excess of several meters above mean sea level (Wang et al. 2014). Added on top of the effect of storm surge, tropical cyclones often produce some of the highest waves recorded. For example, in the Gulf of Mexico, single waves were recorded up to 27 m during Hurricane Ivan, 2004 (Wang et al. 2005)

Several studies made significant progress in anticipating future impacts of sea-level rise during severe storm events, with some focusing on the application of discrete modeling (Mousavi et al. 2010; Woodruff et al. 2013; Walsh et al. 2016; Passeri et al. 2018). Among the most used modeling tools, the XBeach (eXtreme Beach behavior) model was initially developed in response to significant morphological changes to sandy coasts along the eastern seaboard of the USA during the 2004–2005 Atlantic hurricane season (Roelvink et al. 2003; Roelvink et al. 2009). It has since proven to be a highly robust model as it incorporates a 2DH (depth-averaged) coupled hydrodynamic and morphodynamic architecture, which allows to properly simulate small-scale coastal environments during short-duration high-energy events. XBeach is open-source and has been used in many studies focusing on the modeling of future tropical cyclone impacts on sandy coastlines and barrier islands. Most recently, Passeri et al. (2018) have modeled the potential impact of sea-level rise under tropical cyclone conditions on low-lying uninhabited sections of sandy barriers along the Gulf coast. However, human development along the coastline is expected to increase in the future, placing greater pressure on coastal planners to provide adequate protection (Small and Nicholls 2003). This requires the investigation of future changes in morphodynamics and hydrodynamics along unnatural, anthropologically controlled, and managed coastlines.

In this study, we use XBeach to investigate how a managed coastline in Palm Beach County, FL, will respond to the same tropical cyclone (Hurricane Matthew, October 2016) under different sea-level projections. We first use a model run under current sea level as a baseline for comparison, then we investigate how coastal morphology, wave, current velocities, and land inundation would change under two sea-level scenarios: one representing a classic

sea-level projection following a worst-case IPCC scenario (RCP8.5, Hausfather and Peters 2020), the other one including to the previous a significant Antarctic ice sheet collapse (DeConto and Pollard 2016).

Materials and methods

Study area

Florida is an ideal test area to study how the combined effect of a tropical storm and rising seas would affect a well-developed coastline. Along the coasts of Florida, in fact, there is an almost unique convergence of human development, sea level rise, and tropical cyclone risks. Maloney and Preston (2014) showed that Florida would experience a 13% increase in inundated area under a 0.82 m sea-level rise scenario. At particular economic risk is the residential housing market in these areas which, besides the immediate threat of destruction during a tropical cyclone, experiences property value loss due to frequent near-by coastal and or property flooding. For example, McAlpine and Porter (2018) calculated that in Miami-Dade County, FL, the residential home market has lost \$465 million in value between 2005 and 2016. This figure is poised to increase further in the coming decades.

In early October 2016, Hurricane Matthew, a Category 4 hurricane on the Saffir-Simpson scale, passed within 70 km of Palm Beach, FL (Figure 1a, Stewart 2017). Matthew spread tropical storm force winds across most of the southeast coast of the USA. Maximum storm surge height along the southeastern coast ranged between 2.35 and 1.8 m, with maximum inundation in Florida reaching 1.95 m above Mean Higher High Water (MHHW). While the eyewall of the storm tracked northward offshore of Florida, a combination of storm surge, strong wave action, and high tides caused widespread beach and dune erosion. In Palm Beach County, this totaled more than \$29 million, out of the estimated total $\$10 \pm 2$ billion in damage to the USA caused by Hurricane Matthew (Stewart 2017).

Model setup

We use XBeach (Roelvink et al. 2003; Roelvink et al. 2009) to simulate waves and storm surges caused by Hurricane Matthew on a sector of the Florida coast under different sea-level scenarios. Here, model input is derived by combining LiDAR topo-bathymetric data from the US Army Corps of Engineers (USACE) with non-erodible and variable Manning roughness layers. As boundary conditions, we use

the storm surge measured at Lake Worth Pier tide gauge, and wave parameters from WAVEWATCH III (Fig. 1a, d). We run our model first under modern sea level [hereafter, Baseline model]. We then run the model under the localized sea-level projections extracted by Kopp et al. (2014) [hereafter, K14] and Kopp et al. (2017) [hereafter, K17] at the Miami Beach (Florida) tide gauge (Fig. 1c). Both K14 and K17 are compared with the Baseline model.

Our model utilizes an irregular, rectilinear grid covering 5 km long-shore and 3 km in the cross-shore. Grid resolution increases in a step wise manner from the offshore (15 m), nearshore (8 m), onshore (1 m), and decreases again in the back-barrier lagoon (8 m). All grid lines intersect at 90° angles and the overall grid is rotated clockwise 2° from north to provide the best perpendicular intersection to the coastline. Model run time was set to 96 h, encompassing the build-up of storm surge and the re-adjustment of water level following the storm (Fig. 1d). To reduce computation load, XBeach utilizes a morphological factor (morfac). This factor accelerates the morphological development over fewer time-steps. In our model runs, morfac was set to 10, thereby multiplying each bed-level update by 10.

Offshore and back-barrier lagoon hydrodynamic boundaries are all set to absorbing-generating (weakly-reflective). The right and left boundaries are set to Neumann-style (the XBeach default). Neumann boundaries allow no change in water surface level or velocity between the boundary cell and the “cell” beyond the model domain. This can result in some variance in morphodynamic change in the cells immediately adjacent to the boundary and is here addressed by not considering model results within 1 km of the boundary during post-processing.

To resolve the overall wave environment, our model set-up utilizes a single parametric spectrum defined in a JONSWAP file. Waves generated from the JONSWAP file are then propagated throughout the model using the surf beat mode in XBeach. Here, the wave heights of short-waves are calculated in the wave group scale (Roelvink et al. 2009). The surf beat mode enables the inclusion of wave-driven currents, infragravity waves, and infragravity swash (McCall et al. 2010). This is achieved through the summation of the interacting wave energies and leads to a decrease in the overall grouping of waves (Roelvink et al. 2003; Roelvink et al. 2009; McCall et al. 2010; Daly et al. 2012; McCall et al. 2015; Passeri et al. 2018). Shallow water wave breaking was calculated using the wave breaking formula derived in Daly et al. (2012). Here, the wave breaking and reforming is controlled by the ratio between short-wave height to water depth thereby dictating either a breaking or reforming limiter, γ_b and γ_r respectively.

Input data

Topo-bathymetry, bed-friction, and sediments

As initial topography, we used the topo-bathymetric LiDAR dataset collected by the USACE at the end of May 2016 (Fig. 1b). We characterized the land cover of the study area using shapefiles from both Florida State and local Palm Beach County governmental agencies. Building foundations, parking lots, tennis courts, and other large expanses of concrete were rendered and added to a digitized database of the island’s road network. Coastal defense structures along both sides of the island, including several stone groins and a vertical concrete seawall backing the beach along much of the island, were also digitized. We extracted foliage from the pre-storm LiDAR utilizing the “Auto-Classify Buildings and Vegetation Points” tool within Globalmapper (v.18). We then treated the center of each resulting foliage polygon as an individual tree trunk, created a buffer of 2 m around each tree to represent their root balls and added to the non-erodible layer. Upper beach areas were mapped from aerial photographs and an offshore patch reef was digitized manually from satellite imagery (Finkl et al. 2008).

The mapped ground features were then summarized into five main categories, to which we assigned bed friction following the Manning values recommended by NOAA (Table 1). Manning values range between 0.03 $s/m^{1/3}$ for bare land and 0.17 $s/m^{1/3}$ for dense foliage. The offshore reef was assigned a Manning value of 0.05 $s/m^{1/3}$. In conjunction with bed friction, XBeach allows for the inclusion of a non-erodible scheme for onshore development as well as nearshore coastal protection structures. This is enabled by the assignment of an erosional depth for each grid node. In this case, we set hardened structures (roads, buildings, etc.) to 0 m while all other areas have a sediment depth of 50 m, effectively allowing for erosion during the model run. Sediment characteristics,

Table 1 Manning values based on land use classification derived from NOAA’s Coastal Change Analysis Program (C-CAP) 2010

Land usage	Manning value ($s/m^{1/3}$)
Urban Development	0.12
Open space	0.035
Bare land	0.03
Mixed forest	0.17
Open water	0.03

including grain size, were derived from the works of Blott and Pye (2006), Dean et al. (1997), Phelps et al. (2009), and Soulsby (1997), with averaged particle size values of D90: 0.6 mm, D60: 0.3 mm, and D15: 0.2 mm. These grain size values were applied as constant throughout the entire model domain.

Hydrodynamic boundary conditions.

Storm surge data was extracted from Lake Worth Pier (PSMSL Station # 1696, Permanent Service for Mean Sea Level (PSMSL) 2019), and assigned at the offshore boundary as water level forcing (Fig. 1d). We remark that,

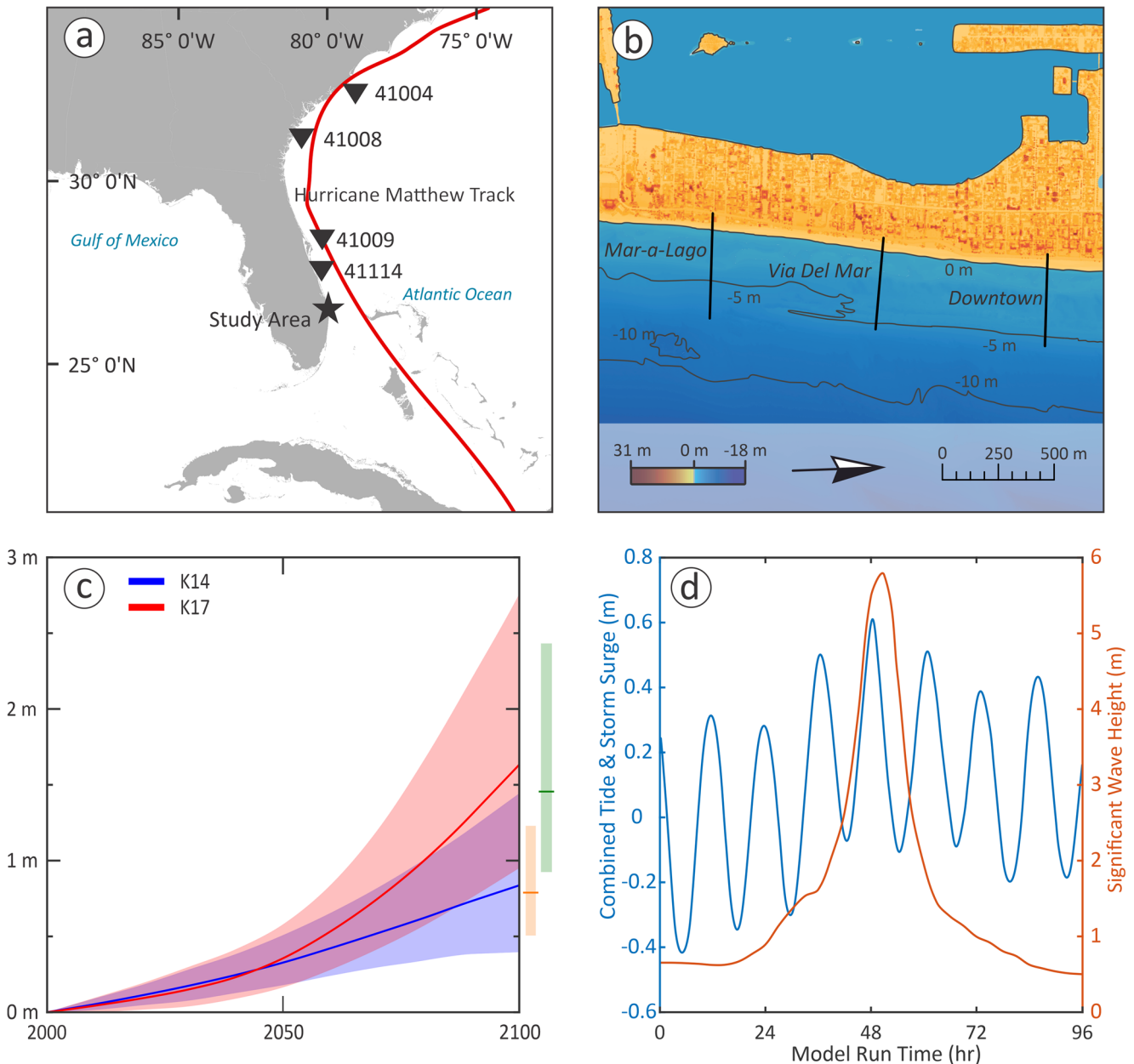


Fig. 1 (a) Overview map indicating the track of Hurricane Matthew. Inverted black triangles show the four buoys that were used by NOAA for WAVEWATCH III validation. (b) Excerpt of pre-storm nearshore topography and bathymetry overlaid with cross-beach profiles used for analysis. (c) Sea-level rise scenarios from Kopp et al. (2014) [K14, +0.84 m SLR] and Kopp et al. (2017) [K17, +1.62 m SLR] for Miami

Beach Tidal Gauge under RCP 8.5. Solid line represents the median and shaded area is the 5-95 % confidence interval. Global mean sea levels extracted from K14 (yellow) and K17 (green). (d) Combined tidal stage and storm surge (blue) plotted with significant wave height (orange) during the model run

while this station is outside of the model domain, the gauge is located 9 km to the southeast of the study location on the oceanside of the island. The observed storm surge was 0.5 m above the predicted tidal stage. Depending on the sea-level scenario, we added the 2100 sea-level rise to the water level input. Sea-level scenarios were extracted from open-source MATLAB scripts compiled by Kopp et al. (2014) and (Kopp et al. 2017). As no MATLAB ensemble for Lake Worth Pier exists, we utilize values generated from Miami Beach (PSMSL Station # 363, Permanent Service for Mean Sea Level (PSMSL) 2019). This choice is justified by the fact that the underlying geology and land use at this site are similar to those of Palm Beach. We chose to model the sea-level projections corresponding to the RCP 8.5 emission scenario (popularly termed “business as usual”, but recently labeled as “worst-case”). Using the tools described above, we generated a localized mean sea-level rise of 0.84 m and 1.62 m, K14 and K17 respectively, that we added to the water level in our different model runs (Fig. 1c).

The nearest buoy to the study area (Fort Pierce Buoy # 41114, National Oceanic and Atmospheric Administration 2019) was cast adrift during the peak of Hurricane Matthew, leaving an incomplete wave record at this station. Therefore, input wave data for the model is derived from WAVEWATCH III (Tolman 2009). The model utilizes 4-minute resolution hydrodynamic data derived from the Gulf of Mexico to NW Atlantic grid. WAVEWATCH III skill (i.e. model/data comparisons) reports for the surrounding buoys are continuously generated by NOAA, and showed strong prediction capability of significant wave height during Matthew. WAVEWATCH III data show that, at the offshore boundary of our model, peak significant wave height (H_{rms}) and period (T_p) were 5.9 m (Fig. 1d) and 11.4 s, respectively. We highlight that in our model runs, we do not modify the intensity of the modeled tropical cyclone to account for a potential increase in tropical cyclone intensity under a future warmer climate. On this matter, the IPCC AR5 (Hartmann et al. 2013) states that it is “virtually certain that the frequency and intensity of the strongest tropical cyclones in the North Atlantic has increased since the 1970s”, but there is still low confidence in future tropical cyclone projections (e.g. Walsh et al. 2016; Wehner et al. 2019).

Model validation

Our model validation is reliant upon the limited data available post-Matthew. Therefore, we compare the model computed bed-level change under modern conditions with a post-storm topo-bathymetric LiDAR survey carried out by the U.S. Geological Survey (USGS) in the aftermath of Hurricane Matthew (Fig. 2). We highlight that, while this is the only possible validation strategy for our model, it is not

ideal. To compare the post-storm LIDAR with the bed-level changes modelled in our Baseline run, we sampled bed level changes using a 5 m × 5 m grid divided into two regions: maximum inundation to mean sea level (onshore, Fig. 2b) and mean sea level to the estimated depth of closure, 10 m (nearshore, Fig. 2a). The actual depth of closure based on wave data over the last 5 years from near-by NOAA Bouy #41114 is calculated after (Hallermeier 1981) at 7.35 m. Initial rudimentary comparison between the Baseline and post-storm LiDAR shows a mean difference of 0.076 ± 0.37 m. Our formal validation computation is adapted from McCall et al. (2015) and Gallagher et al. (1998) and utilizes a measure for skill and is calculated via the following equation:

$$Skill = 1 - \frac{\sum_{i=1}^N (\Delta Z_{LiDAR} - \Delta Z_{XBeach})^2}{\sum_{i=1}^N (\Delta Z_{LiDAR})^2} \quad (1)$$

where δZ_{LiDAR} and δZ_{XBeach} represent the bed-level change (sedimentation and erosion) calculated in the post-storm LiDAR and XBeach model output respectively. Bias was then calculated using:

$$Bias = \frac{1}{N} \sum_{i=1}^{10} (z_{bXBeach} - z_{bLiDAR}) \quad (2)$$

so as $Z_{bXBeach}$ and Z_{bLiDAR} represent the final bed-level of the XBeach model and post-storm LiDAR respectively. For model skill, one represents a perfect model fit, zero indicates the model is no better than predicting zero bed level change, and a negative skill shows that the model is worse than predicting zero bed level change (Gallagher et al. 1998; McCall et al. 2010). Following this analysis we calculate that the onshore model skill is 0.43 and its bias is -0.08 m (Fig. 2b). Nearshore model predictive performance is worse, with a skill of -0.01 and a bias of -0.03 (Fig. 2a).

Limits of the Palm Beach model

Within this model workflow, several assumptions are made that limit the reliability of the results. First, our topo-bathymetric input predates Hurricane Matthew. Therefore, it is highly possible that the initial bed level we use in the model is different from the real-world initial bed-level prior to the tropical cyclone (e.g. Plant et al., 1999; McCall et al. 2010). To examine whether significant changes may have occurred between May 2016 and October 2016 (when Hurricane Matthew hit the study area), we performed a qualitative analysis of normal beach morphological conditions. Aerial photographs of Palm Beach from September–October of previous years (2010, 2013, 2015, and 2017) show the approximate geometry and extent of the nearshore bar. Although the geospatial position of the beach bar varies, the overall geometry is consistently

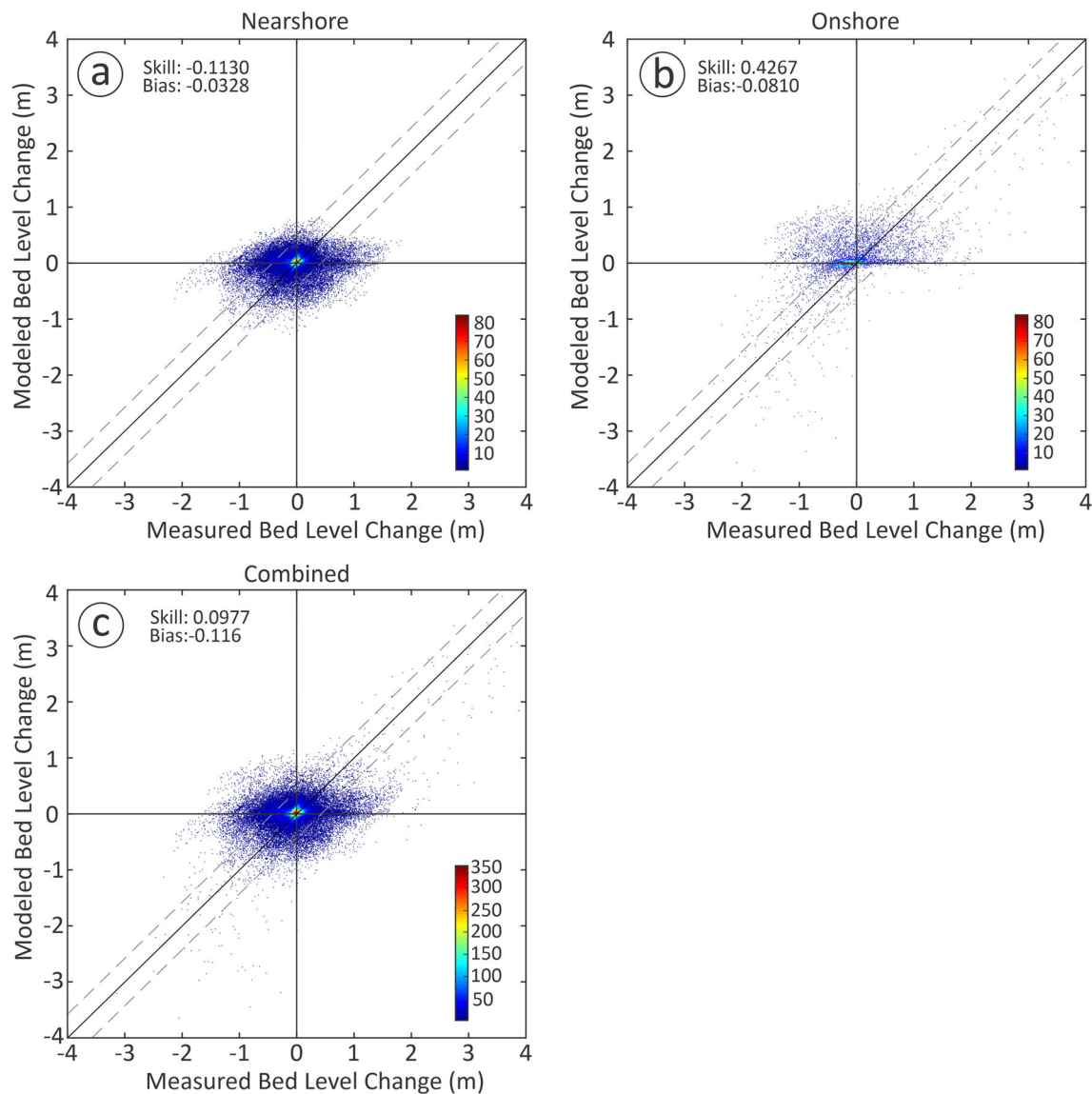


Fig. 2 Resulting Model nearshore bed level change compared to LiDAR nearshore bed level change heat maps, where the ideal 1:1 relationship between model and actual is highlighted by the solid diagonal line. The 2σ is included by the dashed diagonal lines. Nearshore (a) is

shore-parallel in the late summer and early fall. However, the initial bed level indicates an irregular, curved geometry. This short analysis gives confidence that the LiDAR dataset we used as topographic input does not contain significant artifacts due to the seasonality of coastal processes in the study area.

Secondly, the model runtime does not continue until the post-LiDAR survey was conducted, allowing time for swell from the remnants of Matthew as well as swell from the central-Atlantic Hurricane Nicole to interact with the study area and drive potential nearshore change (Hegermiller et al. 2019). The shortcoming introduced by the interlude

from MSL to the assumed closure depth. Onshore (b) is between maximum inundation and MSL. Combined (c) represents points between maximum inundation and 10 m depth.

between pre- and post-LiDAR is partially addressed by our choice of comparing the future sea-level scenarios with the Baseline model. As the only parameter changing between model runs is the added sea-level rise, we are confident that the relative differences between model runs are less biased than the absolute values given as output.

The third limitation of our modelling approach resides in the fact that we run our models for 96 h, during which each sea level scenario is added linearly to the tide and storm surge for the entire duration of the model. As our sea level scenarios represent 2100 levels, to adhere to reality we would need to model 80 years of coastal

processes before running our tropical cyclone simulation (Enríquez et al. 2019). Nevertheless, the importance of this response will depend on the level of management that the coast is subject to. Recent local authorities report that the coastal management approach at Palm Beach (i.e. beach nourishment and armoring) is not expected to drastically change in the foreseeable future (Palm Beach County Department of Environmental Resources Management 2014). If this coastline will remain managed as it is today and no significant island abandonment occurs (Arenstam Gibbons and Nicholls 2006), the amount of overall deviation from the modern beach geometry will be limited through time.

Finally, our hydrodynamic regime for each scenario is largely dictated by the linear storm surge and sea-level input at our boundary water level. In large-scale hydrodynamic models, this assumption has been shown to not be representative as sea-level rise has the potential to influence both storm surge (Bilskie et al. 2014) as well as near-shore wave heights non-linearly (e.g., Melet et al. 2018; Vousdoukas et al. 2017). However, in order to determine a representative non-linear increase to our

offshore water level in both scenarios, the model presented here would need to be nested within a basin circulation model, similar to Bilskie et al. (2014), and would therefore require significantly more computational capability.

Results

In the following sections, we present our results dividing our model domain into three representative areas, named after nearby landmarks: *Downtown*, *Via Del Mar*, and *Mar-a-Lago*. These can be located within the study area in Fig. 1b. Comparing the Baseline model run with K14 and K17 scenarios, we describe how changes in sea-level affect coastal morphology, nearshore hydrodynamics, and the inundation of coastal properties in the three representative areas.

Morphological change

Both K14 and K17 simulations show that, in comparison with the Baseline model, sedimentation and erosion

Fig. 3 Sedimentation and erosion for each representative area within the model domain. The sedimentation and erosional values show the change from the modern scenario. The initial shoreline is represented the respective scenario's 0-m water depth contour (i.e., MSL). Grey polygons represent the non-erodible layer as set in each XBeach simulation. (a–c) model run under K14 sea-level scenario [+0.84 m SLR]. (d–f) Model run under K17 sea-level scenario [+1.62 m SLR]. The black lines represent the transects shown in Fig. 3

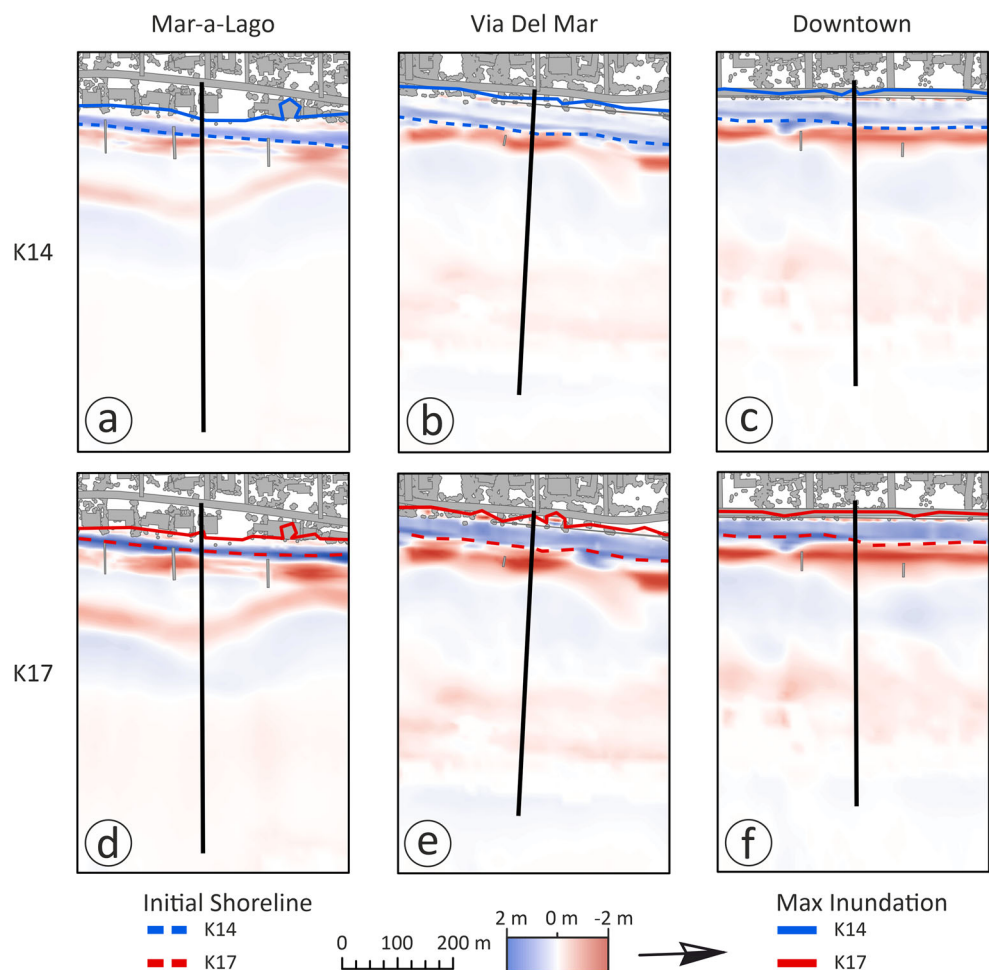
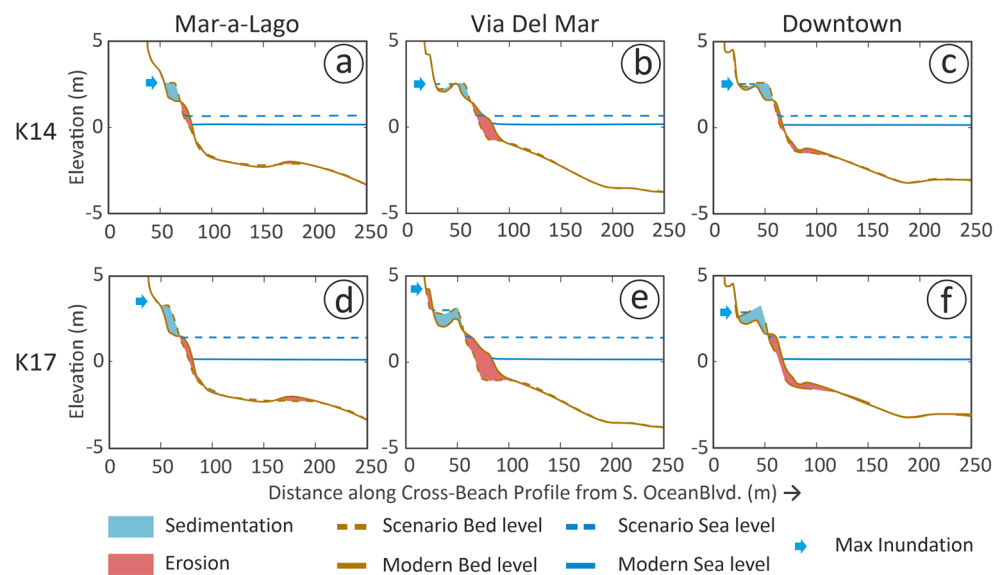


Fig. 4 K14 [+0.84 m SLR] (a–c) and K17 [+1.62 m SLR] (d–e) final bed level in comparison to the modern final bed-level. Overall differences between the resulting two bed levels are highlighted in blue for sedimentation and red for erosion. Post-storm water level and maximum inundation are shown for each scenario at each cross-beach profile (blue arrows)



generally increase in both spatial extent and intensity with higher sea level (Figs. 3 and 4).

The south of the model domain (*Mar-a-Lago* Fig. 3a, d) is characterized by an initial narrow, 21 m wide beach backed by low-lying vegetated dunes in front of residential properties, making this section of coastline more vulnerable to inundation. Under K14, this is made apparent as maximum inundation reaches past this dune line and onto the beachfront properties (Fig. 3a). This impact is amplified under K17 scenario, with more pronounced overwash deposits on the beach in conjunction with greater maximum inundation and foreshore retreat (Fig. 4d).

Moving north (*Via del Mar*, Fig. 3b, e), the beach becomes wider, and is without groin protection. Unlike *Mar-a-Lago*, the beach backs up against a 1.5-m-high sandy berm, before a seawall. During K14, erosion becomes more continuous than in the *Mar-a-Lago* section. Inundation reaches the seawall for most of the profile. Under K17, inundation dramatically extends onshore, overtopping the seawall, and leads to the flooding of adjacent coastal properties (Fig. 4e). Similarly, under K17 erosion is continuous, and increases in intensity, principally with the significant retreat of the foreshore toe and narrowing of the beach profile when compared to both K14 and especially the Baseline model (Fig. 3e).

Further north (*Downtown*, Fig. 3c, f), the narrow (45 m wide) beach is reinforced with groins and a seawall backing up to the City of Palm Beach. Under K14, this area experiences moderate increases in erosion as well as overwash deposits along the beach toe, when compared to the Baseline model. This forces the foreshore to dramatically retreat as well as steepen when compared to what happens under modern sea level. As sea level increases

under K17, both the sedimentation and erosion along the beach becomes more continuous and more pronounced (Fig. 4f). Both K14 and K17 erode the sediment at the base of the seawall to approximately the same extent, slightly more than under modern conditions (Fig. 4).

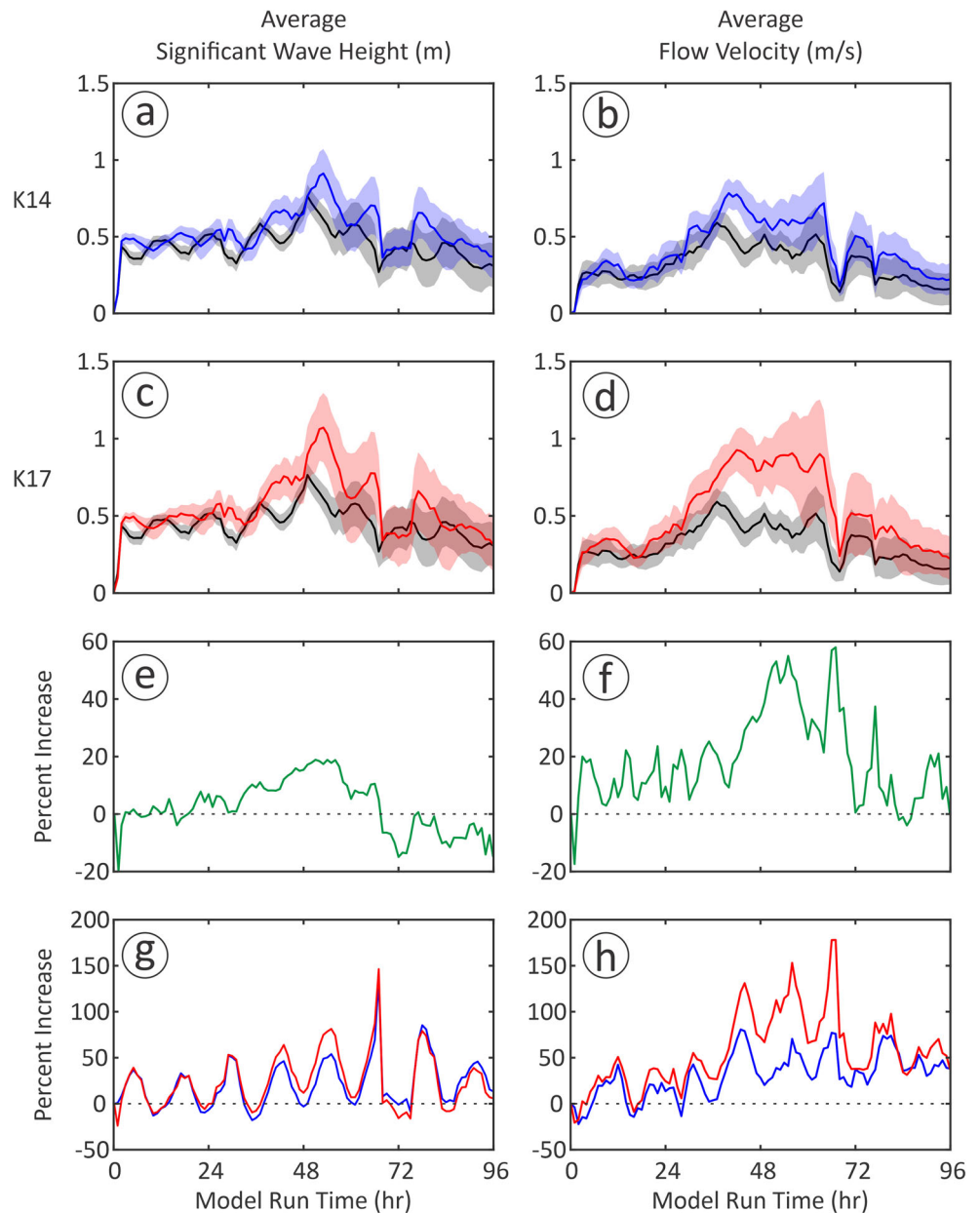
The stark increase of erosion from K14 to K17 across much of the model domain is further highlighted by the increased volume of sediment movement within the model domain. When comparing the volume change between the Baseline and K14, a dramatic increase in sediment movement emerges, with 56,835 m³ more in eroded sediment. Sediment dynamics intensify even further under K17. Under the highest sea-level tested, volume change compared to the baseline model show an even further increase of 83,119 m³.

Change of nearshore hydrodynamics

From our model runs, we extract wave height and flow velocity hourly along the surf zone (1-m water depth contour) for each scenario. This allows us to compare hydrodynamic conditions across the same time intervals for different sea-level scenarios. In Fig. 4, we show the mean and standard deviation envelope of wave height and flow velocity for each scenario, the percentage change between K14 and K17, as well as the percentage change between each scenario and the Baseline model.

Pre-storm waves (0- to 24-h model run time, Fig. 5) are similar under modern, K14 and K17 sea levels (0.5 m significant wave height). At approximately 40 h run time, mean significant wave height of both K14 and K17 rise above the modern scenario. Here, mean significant wave height reaches a maximum of 1.12 m and 1.34 m, for K14

Fig. 5 Nearshore Hydrodynamics sampled along the 1-m water depth contour interval (surf zone). Solid lines in (a) and (c) show the average significant wave height under, respectively, K14 and K17 scenarios. Shaded areas represent 1 standard deviation. Black line and gray shaded areas show the Baseline model results, for comparison. (b) and (d) same as (a) and (c), but for average flow magnitude. (e) and (f) show the percentage increase between K17 and K14 for, respectively, average significant wave height and flow velocity. (g) and (h) show the percentage increase of, respectively, average significant wave height and flow velocity computed between K14 (blue), K17 (red) and the Baseline model.



and K17 respectively. Mean flow velocity follows the same trajectory as significant wave height (Fig. 5). Under both K14 and K17, the mean flow velocities begin to diverge from the Baseline model after its peak of 0.6 m/s at the 37-h time step. In both future scenarios, mean flow velocity climbs to peak values 0.78 m/s and 0.93 m/s respectively, by approximately 40-h model run time. Flow velocities stay elevated for the following 24 h before decreasing to pre-storm levels.

In order to more tangibly understand the overall impact of sea-level rise and storm surge, we present the percentage increase in flooded properties under the current management regime. To do this, we adopted the property inundation evaluation method from McAlpine and Porter

(2018) to our post-storm inundation. While inundation due to King Tides and other recurring events have a continuous and immediate impact, storm surge caused by tropical cyclones greatly enhances inundation (Stewart 2017).

According to the property parcel database provided by (Palm Beach County Information System Services 2020), there are 383 properties within our model domain. Here, we consider a property with at least one wetted model cell as inundated, resulting in a striking difference among the different sea-level scenarios. While only 4% of properties are inundated in our Baseline model, in K14 and K17 scenarios this value increases to 27% and 58%, respectively (Fig. 6). Moreover, inundated roads are also considered as having a drastic effect on property value (McAlpine and

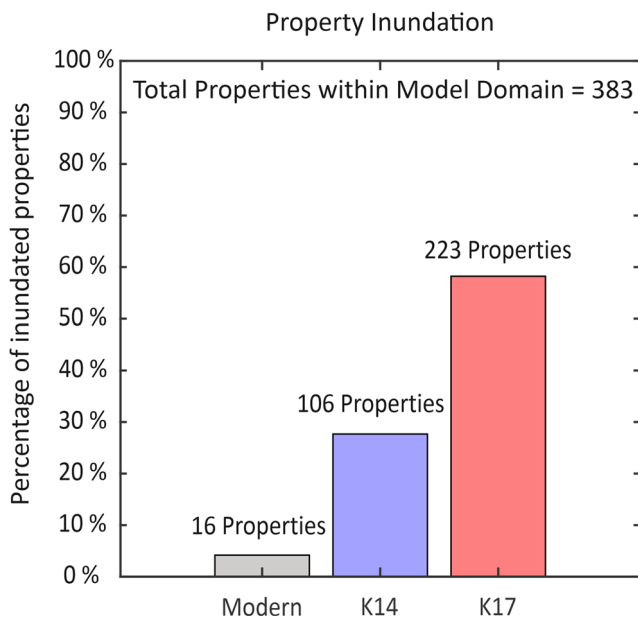


Fig. 6 Percentage of properties within the model domain experiencing inundation during Hurricane Matthew under each sea level scenario

Porter 2018). Considering any wetted cell within a road boundary as an inundated surface, we calculate that over 99% of properties within our model domain are within 250 m of an inundated road under K14, compared to from 11.7% under modern sea level. The K17 scenario shows 100% of properties experiencing nearby flooded roads. It should be noted that the property database (Palm Beach County Information System Services 2020) and road boundaries (see “[Topo-bathymetry, bed-friction, and sediments](#)”) used within this analysis were not resampled within the model grid environment. However, this should not drastically alter the increase of flooded properties with respect to increased sea level, nor should it dramatically change the number of flooded roads on the island.

Discussion

From our results, we calculate that shifting sea level to projected values under K14 and K17 sea-level conditions pushes wave runup and overwash to, or almost to, the seawall along most of the model domain. This in turn increases mean significant wave height during the entire model run under K14 an average of 21% compared to the modern baseline, and to 25% under K17. During the storm, the peak mean significant wave height increases 19% under K14 and 40% under K17 (Fig. 5g). This increase in mean significant wave height is unsurprising as increasing the apparent water depth delays wave breaking, moving the surf zone closer to shore (e.g. Battjes and Groenendijk 2000). Looking at the relative differences between modeled

waves in K14 (without AIS collapse) to K17 (with AIS collapse), peak storm conditions show a 21% increase (Fig. 5e).

As significant wave height increases, so too does the surf zone flow velocity. While significant wave height experiences a peak as the height of the storm reaches the model boundary (Fig. 1d), mean flow velocity peaks and then plateaus for 24 h (Fig. 5b,d). Under K14, mean flow velocity increases 31% from modern, while K17 increases 57% on average. During the peak of the storm, flow velocities increase 79% under K14 and to over 130% under K17 (Fig. 5h). With this increase, the swash zone increases, allowing for greater sediment mobilization to occur (e.g. Masselink and Russell 2006; van Rijn 2009).

As sea level is increased in our simulation, overwash becomes much more prevalent, as the swash zone widens. Along much of the model domain, the beach becomes awash during the storm. In a natural system, this excess water would flow over the island (overwash) and create washover fans, depositing the eroded material on the lagoon side of the barrier (Jiménez et al. 2006; Donnelly 2007). However here, much of the beach is backed by seawalls and landward propagation to the overwash is halted (Fig. 4). Once the landward flow is halted, sediment at the foot of the seawall is suspended, creating a scour and is then subsequently carried to the nearshore (Nederhoff 2014). This rearrangement of beach sediment under intensified conditions leaves the coast more narrow, and therefore more vulnerable to subsequent storms (Eichentopf et al. 2019). Additionally, increases in sediment redistribution within the study area are also highlighted by this, with the K17 scenario showing an increase of 46% in total eroded volume when compared to K14.

In our simulations, during the peak of the storm, overwash regularly reaches the seawall at *Via Del Mar* and *Downtown*. Under both K14 and K17, the seawall is consistently overtopped during Matthew. This is not the case under simulated modern sea level conditions, where seawall overtopping is rare and inundation of the immediate beach front properties seldom occurs (4% of properties within the model domain). However, under K14, inundation increases to 27% and then further to nearly 60% of properties under K17. As a comparison, Maloney and Preston (2014) calculate that housing exposure to inundation increase along the US Gulf and Atlantic coasts is between 83% and 230%. Our numbers are not as quite as alarming, but they indicate a clear difference in flooded properties according to different ice melting scenarios (30% more flooded properties in K17 vs K14). Of note is that greater inundation is not only an issue with immediate impacts (e.g. damage to residential properties), but also influences coastal property value and the economic prosperity for the region in the long term (McAlpine and Porter 2018).

Conclusion

This study focuses on how one of the most valuable coastal areas globally would be affected by a tropical cyclone under extreme future sea level scenarios. Conditions observed during Hurricane Matthew along the Florida coast are representative of what might be experienced during a pass-by event. This is a more common scenario, for many coastal areas, than a tropical cyclone making direct landfall or the field of maximum wind passing directly offshore. Using a 2DH hydrodynamic and morphodynamic coupled XBeach model, we show how a managed shoreline might be affected, under the “worst case” Representative Concentration Pathway 8.5, by a tropical cyclone analogous to Matthew under both IPCC-like [K14] and enhanced future Antarctic melting [K17] scenarios. While localized to our study area, our results point to two main conclusions that may be generalized to other similar areas:

1. Under future sea level scenarios, our model runs predict an increase of significant wave height and flow velocities directly at the shore. This, in turn, leads to changes in the sediment budget, with an increase of 46% in eroded volume between K14 and K17. As well as a significant increase of property and infrastructure inundation under higher sea level scenarios.
2. Even within the two extreme scenarios adopted here, the intensity of wave and flow, sediment mobilization, and subsequent property inundation are significantly increased when a scenario including enhanced Antarctic ice sheet melting is considered.

While Hurricane Matthew did not make landfall at Palm Beach, our results suggest that future sea-level rise has the potential to transform moderate storm conditions into a major event. From a coastal management perspective, this underscores the urgency of understanding how future sea-level rise will be exacerbated by Antarctic ice-shelf and ice-cliff instability.

Acknowledgements This paper is the product of PB’s Master Thesis at the University of Bremen. The non-erodible shapefile was digitized by Marco Tack. Jürgen Pätzold (University of Bremen) provided constructive feedback during project development as well as during manuscript review. Contents from this paper were presented at the following conferences: iSLR (Utrecht, 2018), EGU (Vienna, 2019), and INQUA (Dublin, 2019). The authors acknowledge PALSEA (a PAGES / INQUA) working group for useful discussions/comments at the 2019 meeting (Dublin, Ireland, 21–23 July 2019).

Funding Open Access funding enabled and organized by Projekt DEAL. This research was financially supported by the Institutional Strategy of the University of Bremen, funded by the German Excellence Initiative (ABPZuK-03/2014).

Declarations

Author contribution PB, AR, and EC developed the project. PB performed all model runs with EC and CD providing advice and input on model parameters. The initial manuscript was written by PB and has been revised and approved by all authors.

Data availability Model param files and inputs are available on GitHub at: https://github.com/pboyden/Palm_Beach_XBeach.

Declarations

Competing interests The authors declare no competing interests.

Open Access This article is licensed under a Creative Commons Attribution 4.0 International License, which permits use, sharing, adaptation, distribution and reproduction in any medium or format, as long as you give appropriate credit to the original author(s) and the source, provide a link to the Creative Commons licence, and indicate if changes were made. The images or other third party material in this article are included in the article’s Creative Commons licence, unless indicated otherwise in a credit line to the material. If material is not included in the article’s Creative Commons licence and your intended use is not permitted by statutory regulation or exceeds the permitted use, you will need to obtain permission directly from the copyright holder. To view a copy of this licence, visit <http://creativecommons.org/licenses/by/4.0/>.

References

- Arenstam Gibbons Sj, Nicholls RJ (2006) Island abandonment and sea-level rise: an historical analog from the Chesapeake Bay, USA. *Glob Environ Chang* 16(1):40–47. <https://doi.org/10.1016/j.gloenvcha.2005.10.002>
- Battjes JA, Groenendijk HW (2000) Wave height distributions on shallow foreshores. *Coast Eng* 40(3):161–182. [https://doi.org/10.1016/S0378-3839\(00\)00007-7](https://doi.org/10.1016/S0378-3839(00)00007-7)
- Bilskie MV, Hagen SC, Medeiros SC, Passeri DL (2014) Dynamics of sea level rise and coastal flooding on a changing landscape. *Geophys Res Lett* 41(3):927–934. <https://doi.org/10.1002/2013GL058759>
- Blott SJ, Pye K (2006) Particle size distribution analysis of sand-sized particles by laser diffraction: an experimental investigation of instrument sensitivity and the effects of particle shape. *Sedimentology* 53(3):671–685. <https://doi.org/10.1111/j.1365-3091.2006.00786.x>
- Daly C, Roelvink J, van Dongeren A, van Thiel de Vries J, McCall R (2012) Validation of an advective-deterministic approach to short wave breaking in a surf-beat model. *Coastal Eng* 60:69–83. <https://doi.org/10.1016/j.coastaleng.2011.08.001>
- Davis JL, Mitrovica JX (1996) Glacial isostatic adjustment and the anomalous tide gauge record of eastern North America. *Nature* 379(6563):331–333. <https://doi.org/10.1038/379331a0>
- Dean RG, Chen R, Browder AE (1997) Full scale monitoring study of a submerged breakwater, Palm Beach, Florida, USA. *Coast Eng* 29(3–4):291–315
- DeConto RM, Pollard D (2016) Contribution of Antarctica to past and future sea-level rise. *Nature* 531(7596):591–7. <https://doi.org/10.1038/nature17145>

- Donnelly C (2007) Morphologic change by overwash establishing and evaluating predictors. *J Coast Res*:520–526
- Edwards TL, Brandon MA, Durand G, Edwards NR, Golledge NR, Holden PB, Nias IJ, Payne AJ, Ritz C, Wernecke A (2019) Revisiting antarctic ice loss due to marine ice-cliff instability. *Nature* 566(7742):58–64. <https://doi.org/10.1038/s41586-019-0901-4>
- Eichentopf S, Karunaratna H, Alsina JM (2019) Morphodynamics of sandy beaches under the influence of storm sequences: Current research status and future needs. *Water Sci Eng* 12(3):221–234. <https://doi.org/10.1016/j.wse.2019.09.007>
- Enriquez AR, Marcos M, Falqués A, Roelvink J (2019) Assessing beach and dune erosion and vulnerability under sea level rise: a case study in the mediterranean sea. *Front Mar Sci* 6:4
- Finkl CW, Becerra JE, Achatz V, Andrews JL (2008) Geomorphological mapping along the upper southeast Florida atlantic continental platform; 1: mapping units, symbolization and geographic information system presentation of interpreted seafloor topography. *J Coast Res* 2008(246):1388–1417
- Gallagher EL, Elgar S, Guza RT (1998) Observations of sand bar evolution on a natural beach. *J Geophys Res Oceans* 103(C2):3203–3215. <https://doi.org/10.1029/97jc02765>
- Hallermeier RJ (1981) Seaward limit of significant sand transport by waves: an annual zonation for seasonal profiles. Report, Coastal Engineering Research Center, Fort Belvoir
- Hartmann D, Tank A, Rusticucci M, Alexander L, Brönnimann S, Charabi Y, Dentener F, Dlugokencky E, Easterling D, Kaplan A (2013) Observations: atmosphere and surface: Climate change 2013 the physical science basis: Working group contribution to the fifth assessment report of the intergovernmental panel on climate change. Cambridge University Press, pp 159
- Hausfather Z, Peters GP (2020) Emissions—the business as usual story is misleading. *Nature* 577(7792):618–620
- Hegermiller CA, Warner JC, Olabarrieta M, Sherwood CR (2019) Wave–current interaction between hurricane matthew wave fields and the gulf stream. *J Phys Oceanogr* 49(11):2883–2900
- Jiménez JA, Sallenger AH, Fauver L (2006) Sediment transport and barrier island changes during massive overwash events. In: *Coastal engineering 2006* (in 5 vol). World Scientific, pp 2870–2879
- Kopp RE, Horton RM, Little CM, Mitrovica JX, Oppenheimer M, Rasmussen DJ, Strauss BH, Tebaldi C (2014) Probabilistic 21st and 22nd century sea-level projections at a global network of tide-gauge sites. *Earth's Fut* 2(8):383–406. <https://doi.org/10.1002/2014ef000239>
- Kopp RE, DeConto RM, Bader DA, Hay CC, Horton RM, Kulp S, Oppenheimer M, Pollard D, Strauss BH (2017) Evolving understanding of antarctic ice-sheet physics and ambiguity in probabilistic sea-level projections. *Earth's Fut* 5(12):1217–1233. <https://doi.org/10.1002/2017ef000663>
- Maloney MC, Preston BL (2014) A geospatial dataset for u.s. hurricane storm surge and sea-level rise vulnerability: development and case study applications. *Clim Risk Manag* 2:26–41. <https://doi.org/10.1016/j.crm.2014.02.004>
- Masselink G, Russell P (2006) Flow velocities, sediment transport and morphological change in the swash zone of two contrasting beaches. *Mar Geol* 227(3–4):227–240
- McAlpine SA, Porter JR (2018) Estimating recent local impacts of sea-level rise on current real-estate losses: a housing market case study in Miami-Dade, Florida. *Popul Res Policy Rev* 37(6):871–895. <https://doi.org/10.1007/s11113-018-9473-5>
- McCall RT, Van Thiel de Vries JSM, Plant NG, Van Dongeren AR, Roelvink JA, Thompson DM, Reniers AJHM (2010) Two-dimensional time dependent hurricane overwash and erosion modeling at santa rosa island. *Coast Eng* 57(7):668–683. <https://doi.org/10.1016/j.coastaleng.2010.02.006>
- McCall RT, Masselink G, Poate TG, Roelvink JA, Almeida LP (2015) Modelling the morphodynamics of gravel beaches during storms with xbeach-g. *Coast Eng* 103:52–66. <https://doi.org/10.1016/j.coastaleng.2015.06.002>
- Melet A, Meyssignac B, Almar R, Le Cozannet G (2018) Underestimated wave contribution to coastal sea-level rise. *Nat Clim Change* 8(3):234–239. <https://doi.org/10.1038/s41558-018-0088-y>
- Mousavi ME, Irish JL, Frey AE, Olivera F, Edge BL (2010) Global warming and hurricanes: the potential impact of hurricane intensification and sea level rise on coastal flooding. *Clim Change* 104(3–4):575–597. <https://doi.org/10.1007/s10584-009-9790-0>
- National Oceanic and Atmospheric Administration (2019) National data buoy center
- Nederhoff K (2014) Modeling the effects of hard structures on dune erosion and overwash: hindcasting the impact of hurricane sandy on new jersey with xbeach. Thesis, Delft University of Technology, the Netherlands
- Neumann B, Vafeidis AT, Zimmermann J, Nicholls RJ (2015) Future coastal population growth and exposure to sea-level rise and coastal flooding—a global assessment. *PLoS One* 10(3):e0118571. <https://doi.org/10.1371/journal.pone.0118571>
- Oppenheimer M, Alley RB (2016) How high will the seas rise? *Science* 354(6318):1375–1377
- Palm Beach County Department of Environmental Resources Management (2014) Palm beach county shoreline protection plan
- Palm Beach County Information System Services (2020) Palm Beach County Open Data. <https://opendata2-pbcgov.opendata.arcgis.com>
- Passeri DL, Bilskie MV, Plant NG, Long JW, Hagen SC (2018) Dynamic modeling of barrier island response to hurricane storm surge under future sea level rise. *Clim Change* 149(3–4):413–425. <https://doi.org/10.1007/s10584-018-2245-8>
- Permanent Service for Mean Sea Level (PSMSL) (2019) Tide gauge data. <http://www.psmsl.org/data/obtaining/>
- Phelps D, Ladle M, Dabous A (2009) A sedimentological and granulometric atlas of the beach sediments of Florida's east coasts. Florida Geological Survey, Tallahassee
- Plant NG, Holman RA, Freilich MH, Birkemeier WA (1999) A simple model for interannual sandbar behavior. *J Geophys Res Oceans* 104(C7):15755–15776. <https://doi.org/10.1029/1999jc900112>
- Pörtner HO, Roberts D, Masson-Delmotte V, Zhai P, Tignor M, Poloczanska E, Mintenbeck K, Alegría A, Nicolai M, Okem A, Petzold J, Rama B, Weyer N (2019) Summary for policy makers IPCC, Geneva
- van Rijn LC (2009) Prediction of dune erosion due to storms. *Coastal Eng* 56(4):441–457. <https://doi.org/10.1016/j.coastaleng.2008.10.006>
- Roelvink J, van Kessel T, Alfageme S, Canizares R (2003) Modelling of barrier island response to storms. In: *Proceedings of Coastal Sediments*, vol 3, pp 1–11
- Roelvink J, Reniers AJHM, van Dongeren AR, van Thiel de Vries JSM, McCall RT, Lescinski J (2009) Modelling storm impacts on beaches, dunes and barrier islands. *Coastal Eng* 56(11–12):1133–1152. <https://doi.org/10.1016/j.coastaleng.2009.08.006>
- Small C, Nicholls RJ (2003) A global analysis of human settlement in coastal zones. *J Coast Res* 19(3):584–599
- Soulsby R (1997) Dynamics of marine sands: a manual for practical applications. Thomas Telford
- Stewart SR (2017) Hurricane matthew. Report, National Oceanographic and Atmospheric Administration
- Tolman HL (2009) User manual and system documentation of wavewatch iii tm (version 3.14). Technical note. MMAB Contrib 276:220
- Törnqvist TE, Wallace DJ, Storms JE, Wallinga J, Van Dam RL, Blaauw M, Derksen MS, Klerks CJ, Meijneken C, Snijders EM (2008) Mississippi delta subsidence primarily caused by compaction of holocene strata. *Nat Geosci* 1(3):173

- Vousdoukas MI, Mentaschi L, Voukouvalas E, Verlaan M, Feyen L (2017) Extreme sea levels on the rise along Europe's coasts. *Earth's Fut* 5(3):304–323. <https://doi.org/10.1002/2016EF000505>
- Walsh KJE, McBride JL, Klotzbach PJ, Balachandran S, Camargo SJ, Holland G, Knutson TR, Kossin JP, Lee Tc, Sobel A, Sugi M (2016) Tropical cyclones and climate change. *Wiley Interdiscip Rev Clim Change* 7(1):65–89. <https://doi.org/10.1002/wcc.371>
- Wang DW, Mitchell DA, Teague WJ, Jarosz E, Hulbert MS (2005) Extreme waves under hurricane Ivan. *Science* 309(5736):896–896
- Wang HV, Loftis JD, Liu Z, Forrest D, Zhang J (2014) The storm surge and sub-grid inundation modeling in New York City during Hurricane Sandy. *J Mar Sci Eng* 2(1):226–246
- Wehner MF, Zarzycki C, Patricola C (2019) Estimating the human influence on tropical cyclone intensity as the climate changes. Springer International Publishing, Cham, pp 235–260. https://doi.org/10.1007/978-3-030-02402-4_12
- Woodruff JD, Irish JL, Camargo SJ (2013) Coastal flooding by tropical cyclones and sea-level rise. *Nature* 504(7478):44–52. <https://doi.org/10.1038/nature12855>

Publisher's note Springer Nature remains neutral with regard to jurisdictional claims in published maps and institutional affiliations.